Statistical approach of nuclear multifragmentation with a realistic nuclear equation of state

S. Mallik*

Physics Group, Variable Energy Cyclotron Centre, 1/AF Bidhan Nagar, Kolkata 700064, India
and Homi Bhabha National Institute, Training School Complex, Anushakti Nagar, Mumbai 400085, India

(Received 6 January 2023; revised 21 March 2023; accepted 1 May 2023; published 15 May 2023)

In this work, the canonical thermodynamical model for nuclear multifragmentation has been updated with a realistic nuclear equation of state. Mass distribution, intermediate mass fragment multiplicity, and isospin sensitive observables have been investigated with a semi-microscopic approach of determining nuclear binding and excitation energies. Production of neutron-rich isotopes as well as isoscaling and isobaric yield ratio parameters have been significantly modified due to inclusion of this realistic nuclear equation of state.

DOI: 10.1103/PhysRevC.107.054605

I. INTRODUCTION

The study of nuclear multifragmentation is important for understanding the reaction mechanism in heavy-ion collisions at intermediate and high energies [1,2]. Nuclear multifragmentation reactions are commonly used study nuclear liquid-gas phase transition [1,3–9] and nuclear equation of state [2,10] and to extrapolate the thermodynamic properties of the astrophysical environment of worm stellar matter from the laboratory scenario [11,12]. Statistical approaches are quite successful for studying nuclear multifragmentation reactions at intermediate energies. The disintegration of excited nuclei are commonly studied by implementing different statistical ensembles. The statistical multifragmentation model proposed by the Copenhagen group [5], the microcanonical models of Gross [13] and Randrup and Koonin [14], and the canonical thermodynamical model (CTM) [15] are widely used. In these statistical models, observables related to nuclear fragment cross section (and/or multiplicity) are usually determined based on the available phase space calculation. Now, to get the accurate phase space, nuclear binding and excitation of all clusters are required and in most of the existing statistical approaches like the canonical thermodynamical model, statistical multifragmentation model, etc., binding is determined from the Bethe-Weizsacker mass formula, which successfully explained the ground-state properties at zero temperature and saturation nuclear density [16,17]. However, nuclear multifragmentation occurs at subsaturation density and higher excitation energy. To include temperature effects in the bulk energy part, the Fermi gas model is commonly used in statistical models of nuclear multifragmentation, and for surface energy part, various additional parametrization in Bethe-Weizsacker mass formula is introduced. The density and/or temperature dependence of the nuclear binding also plays an important role in the study of stellar matter properties and also has significant influence for determining the nuclear properties of extremely neutron-rich and neutron-deficient nuclei formed in multifragmentation reactions.

The aim of this work is to implement more realistic binding and excitation in the canonical thermodynamical model (CTM) for nuclear multifragmentation and to study the impact of it on the basic observables like intermediate mass fragment (IMF) multiplicity, mass distribution, and isospin sensitive observables like isotopic distribution, isoscaling, and isobaric yield ratio. In order to study the decay of the excited fragments produced in the multifragmentation stage, the evaporation model [18] is also updated with the same realistic binding and excitation.

The paper is structured as follows. In Sec. II, a brief introduction of the canonical thermodynamical model is presented. The results are described in Sec. III, and finally a summary and conclusions are discussed in Sec. IV.

II. MODEL DESCRIPTION

In CTM [1,15], it is assumed that statistical equilibrium is attained at the freeze-out stage and the population of different channels of disintegration is solely decided by statistical weights in the available phase space. The calculation is done for fixed mass, atomic number, freeze-out volume, and temperature. In a canonical model [15], the partitioning is done such that all partitions have the correct A_0, Z_0 (equivalently N_0, Z_0). The canonical partition function is given by

$$Q_{N_0,Z_0} = \sum \prod \frac{\omega_{N,Z}^{n_{N,Z}}}{n_{N,Z}!}, \tag{1}$$

where the sum is over all possible channels of breakup (the number of such channels is enormous) satisfying $N_0 = \sum N \times n_{N,Z}$ and $Z_0 = \sum Z \times n_{N,Z}$; $\omega_{N,Z}$ is the partition function of the composite with N neutrons and Z protons and n_{NZ} is its multiplicity. The partition function Q_{N_0,Z_0} is calculated by applying a recursion relation [19]. From Eq. (1), the average number of composites with N neutrons and Z protons can

*swagato@vecc.gov.in

 ©2023 American Physical Society

be expressed as

$$\langle n_{N,Z}\rangle = \omega_{N,Z}\frac{Q_{N_0-N,Z_0-Z}}{Q_{N_0,Z_0}}. \quad (2)$$

The partition function of a composite having N neutrons and Z protons is a product of two parts. One is due to the the translational motion and the other is the intrinsic partition function of the composite:

$$\omega_{N,Z} = \frac{V}{h^3}(2\pi mT)^{3/2}A^{3/2} \times z_{N,Z}(\text{int}), \quad (3)$$

where V is the volume available for translational motion, which can be expressed as $V = V_f - V_0$, where V_0 is the normal volume of nucleus with Z_0 protons and N_0 neutrons. $z_{N,Z}(\text{int})$ is the internal partition function, where the proton and the neutron are fundamental building blocks, and thus $z_{1,0}(\text{int}) = z_{0,1}(\text{int}) = 2$, where 2 takes care of the spin degeneracy. For ^{2}H, ^{3}H, ^{3}He, ^{4}He, ^{5}He, and ^{6}He, $z_{N,Z}(\text{int}) = (2s_{N,Z}+1)\exp[-\beta E_{N,Z}(\text{gr})]$, where $\beta = 1/T$, $E_{N,Z}(\text{gr})$ is the ground-state energy of the composite and $(2s_{N,Z}+1)$ is the experimental spin degeneracy of the ground state. Excited states for these very low-mass nuclei are not included.

A. Conventional approach of determining internal partition function in CTM

In the conventional CTM approach as well as in most of the other statistical models of multifragmentation, for determining the internal partition function of nuclei with $Z \geqslant 3$ the liquid-drop formula is used to calculate the binding energy and the contribution for excited states is taken from the Fermi-gas model. In the CTM approach, the internal partition function is usually expressed as

$$z_{N,Z}(\text{int}) = \exp\frac{1}{T}\Bigg[W_0A - a_s(T)A^{2/3} - a_c^*\frac{Z^2}{A^{1/3}} - C_{\text{sym}}\frac{(N-Z)^2}{A} + \frac{T^2A}{\epsilon_0}\Bigg]. \quad (4)$$

The expression includes the volume energy [$W_0 = 15.8$ MeV], the temperature-dependent surface energy [$a_s(T) = a_{s0}\{(T_c^2 - T^2)/(T_c^2 + T^2)\}^{5/4}$ with $a_{s0} = 18.0$ MeV and $T_c = 18.0$ MeV], the Coulomb energy ($a_c^* = 0.31a_c$ with $a_c = 0.72$ MeV and Wigner-Seitz correction factor 0.31 [5]), and the symmetry energy ($C_{\text{sym}} = 23.5$ MeV). The term $\frac{T^2A}{\epsilon_0}$ ($\epsilon_0 = 16.0$ MeV) represents contribution from excited states since the composites are at a nonzero temperature. In Ref. [20], the volume term of the nuclear binding for extended canonical model is determined from relativistic mean field approach.

B. New approach for determining more realistic internal partition function in CTM

In this work, the internal partition function is determined from a semi-microscopic approach where the Helmholtz free energy of a nucleus with N neutrons and Z protons can be decomposed as [21]

$$F_{N,Z} = F^{\text{bulk}} + F^{\text{surf}} + F^{\text{coul}}, \quad (5)$$

where the bulk part F^{bulk} is originated from bulk nuclear matter at baryonic density $\rho_c = \rho_{c,n} + \rho_{c,z}$ ($\rho_{c,n}$ and $\rho_{c,z}$ are neutron and proton density respectively) and isospin asymmetry $\delta_c = (\rho_{c,n} - \rho_{c,z})/\rho_c = \frac{N-Z}{N+Z}$ occupying a finite spatial volume $V_c = (N+Z)/\rho_c$. The baryonic density with isospin asymmetry δ_c is approximated [22] to the corresponding saturation density (ρ_0) of symmetric nuclear matter at finite asymmetry according to

$$\rho_c(\delta_c) = \rho_0\left(1 - \frac{3L_{\text{sym}}\delta_c^2}{K_{\text{sat}} + K_{\text{sym}}\delta_c^2}\right). \quad (6)$$

Therefore, the bulk part of the Helmholtz free energy given by

$$F^{\text{bulk}} = V_c\left[-\frac{2}{3}\sum_{q=n,z}\xi_{c,q} + \sum_{q=n,z}\rho_{c,q}\eta_q + v(\rho_c,\delta_c)\right], \quad (7)$$

where $\xi_{c,n}$ and $\xi_{c,z}$ are the kinetic energy density of the nucleus due to neutron ($q = n$) and proton ($q = p$) contribution respectively, which can be expressed as $q = n, p$,

$$\xi_{c,q} = \frac{3h^2}{2\pi m_{c,q}^*}\left(\frac{2\pi m_{c,q}^*T}{h^2}\right)^{5/2}F_{3/2}(\eta_{c,q}), \quad (8)$$

where $\eta_{c,q} = F_{1/2}^{-1}\{(\frac{2\pi m_{c,q}^*T}{h^2})^{3/2}\rho_{c,q}\}$ and $F_{1/2}$ and $F_{3/2}$ are the Fermi integrals. The expression of potential energy per particle that can be adapted to different effective interactions and energy functionals is given by

$$v(\rho_c,\delta_c) = \sum_{k=0}^{N}\frac{1}{k!}\left(v_k^{is} + v_k^{iv}\delta_c^2\right)x^k + \left(a^{is} + a^{iv}\delta_c^2\right)x^{N+1}\exp\left(-b\frac{\rho_c}{\rho_0}\right), \quad (9)$$

where $x = \frac{\rho_c-\rho_0}{3\rho_0}$, $a^{is} = -\sum_{k\geqslant 0}^{N}\frac{1}{k!}v_k^{is}(-3)^{N+1-k}$, and $a^{iv} = -\sum_{k\geqslant 0}^{N}\frac{1}{k!}v_k^{iv}(-3)^{N+1-k}$. $N = 4$ and $b = 10\ln 2$ are chosen for this model. This value of b leads to a good reproduction of the Sly5 functional which is used for the numerical applications presented in this paper. The model parameters $v_k^{is(iv)}$ can be linked with a one-to-one correspondence to the usual equation of state (EoS) empirical parameters [23], via

$$\begin{aligned}
v_0^{is} &= E_{\text{sat}} - t_0(1+\kappa_0),\\
v_1^{is} &= -t_0(2+5\kappa_0),\\
v_2^{is} &= K_{\text{sat}} - 2t_0(-1+5\kappa_0),\\
v_3^{is} &= Q_{\text{sat}} - 2t_0(4-5\kappa_0),\\
v_4^{is} &= Z_{\text{sat}} - 8t_0(-7+5\kappa_0),
\end{aligned} \quad (10)$$

$$\begin{aligned}
v_0^{iv} &= E_{\text{sym}} - \tfrac{5}{9}t_0[\{1+(\kappa_0+3\kappa_{\text{sym}})\}],\\
v_1^{iv} &= L_{\text{sym}} - \tfrac{5}{9}t_0[\{2+5(\kappa_0+3\kappa_{\text{sym}})\}],\\
v_2^{iv} &= K_{\text{sym}} - \tfrac{10}{9}t_0[\{-1+5(\kappa_0+3\kappa_{\text{sym}})\}],\\
v_3^{iv} &= Q_{\text{sym}} - \tfrac{10}{9}t_0[\{4-5(\kappa_0+3\kappa_{\text{sym}})\}],\\
v_4^{iv} &= Z_{\text{sym}} - \tfrac{40}{9}t_0[\{-7+5(\kappa_0+3\kappa_{\text{sym}})\}],
\end{aligned} \quad (11)$$

where E_{sat}, K_{sat}, Q_{sat}, and Z_{sat} are saturation energy, incompressibility modulus, isospin symmetric skewness, and

kurtosis respectively and $E_{\rm sym}$, $L_{\rm sym}$, $K_{\rm sym}$, $Q_{\rm sym}$, and $Z_{\rm sym}$ are symmetry energy, slope, associated incompressibility, skewness, and kurtosis respectively. κ_0 and $\kappa_{\rm sym}$ govern the density dependence of the neutron and proton effective mass according to

$$\frac{m_q}{m_q^*(\rho_c,\delta_c)} = 1 + (\kappa_0 \pm \kappa_{\rm sym}\delta)\frac{\rho_c}{\rho_0}, \tag{12}$$

with $q = n, p$. For the applications presented in this paper, all the parameters are taken from the Sly5 functional [24].

The finite-size corrections are included by the surface part of the Helmholtz free energy ($F^{\rm surf}$) [25] for which we adopt the prescription proposed in Refs. [26–28] on the basis of Thomas-Fermi calculations with extreme isospin ratios:

$$F^{\rm surf} = 4\pi r_c^2 A_N^{2/3}\sigma(y_{c,p}, T) \tag{13}$$

with $r_0 = \{\frac{3}{4\pi\rho_0}\}^{1/3}$, $y_{c,p} = Z/(Z+N)$, and

$$\sigma(y_{c,p}) = \sigma_0 h\left(\frac{T}{T_c(y_{c,p})}\right)\frac{2^{p+1}+b_s}{y_{c,p}^{-p}+b_s+(1-y_{c,p})^{-p}}, \tag{14}$$

where σ_0 represents the surface tension of symmetric nuclear matter and b_s and p represent the isospin dependence. For the Sly5 functional, the parameters were optimized in Ref. [26] as $\sigma_0 = 1.09191$, $b_s = 15.36563$, and $p = 3.0$. The temperature dependence is incorporated by

$$h\left(\frac{T}{T_c(y_{c,p})}\right) = \left[1-\left(\frac{T}{T_c(y_{c,p})}\right)^2\right]^2 \quad \text{for} \quad T \leqslant T_c(y_{c,p})$$
$$= 0 \quad \text{for} \quad T > T_c(y_{c,p}). \tag{15}$$

$T_c(y_{c,p})$ is the maximum temperature, for a given value of $y_{c,p}$ up to which a nuclear liquid phase may coexist with the nuclear vapor and its expression in MeV units is given by

$$T_c(y_{c,p}) = 87.76\left(\frac{K_{\rm sat}}{375}\right)^{\frac{1}{2}}\left(\frac{0.155}{\rho_0}\right)^{\frac{1}{3}} y_{c,p}(1-y_{c,p}), \tag{16}$$

where $K_{\rm sat}$ and n_0 are expressed in MeV and fm^{-3} respectively. The Coulomb contribution in Helmholtz free energy is considered as same as before, i.e.,

$$F^{\rm Coul} = a_c^*\frac{Z^2}{A^{1/3}}. \tag{17}$$

III. RESULTS

Statistical model calculations are performed for two fragmenting systems having the same proton number $Z_0 = 75$ but different mass numbers $A_0 = 168$ and 186, which are expected to be formed from the central collision of ^{112}Sn + ^{112}Sn and ^{124}Sn + ^{124}Sn reaction with 75% pre-equilibrium emission [29,30]. The choice of fragmenting systems is based on well-known experiments of ^{112}Sn + ^{112}Sn and ^{124}Sn + ^{124}Sn reactions at 50 MeV/nucleon performed by the MSU group at NSCL [31]. More precise calculation for identifying fragmenting source mass number, isospin asymmetry, and excitation can be found in Refs. [32,33]. As described in Sec. II, fragments with all possible proton numbers

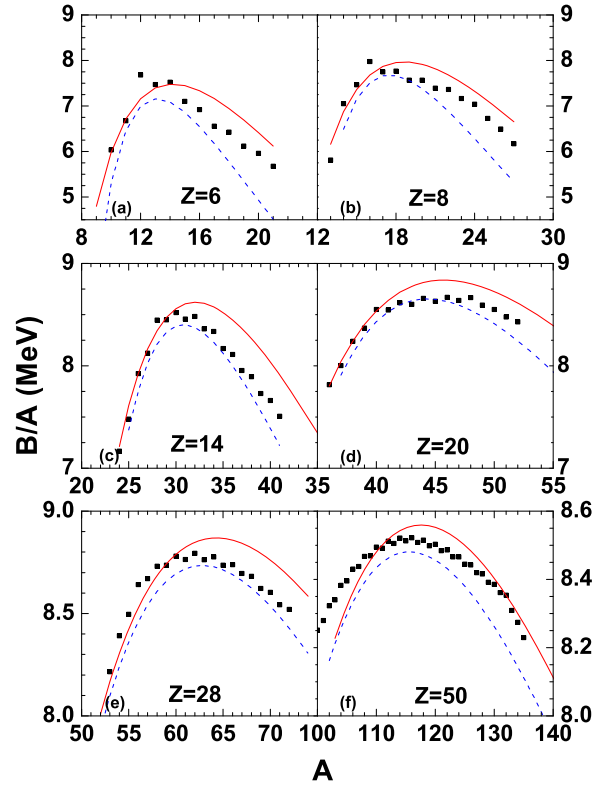

FIG. 1. Binding energy per nucleon of (a) carbon, (b) oxygen, (c) silicon, (d) calcium, (e) nickel, and (f) tin isotopes obtained from nuclear liquid drop model (blue dotted lines) and realistic compressible liquid drop approach with Sly5 parameters (red solid lines). Experimental binding energies taken from AME2020 [34] are shown by black squares.

(i.e., $Z = 1$ to 75) and neutron numbers (within neutron and proton dripline each Z) will be produced in multifragmentation reactions and their multiplicities are linked to the nuclear binding; the binding energies of some selective cases like various isotopes of carbon, oxygen, silicon, calcium, nickel, and tin are shown in Fig. 1. Binding energy per nucleon of the above-mentioned isotopes obtained from the conventional liquid drop model and the more realistic compressible liquid drop approach with Sly5 parameters are compared with their experimental values. From Fig. 1 it can be concluded that the bindings are modified significantly for the neutron-rich nuclei. Neutron-rich nuclei are remarkably produced in multifragmentation reactions, and hence the effect of this binding energy shift on the basic observables of multifragmentation reactions is described below.

Figure 2 represents the mass distribution obtained from CTM calculation with conventional liquid drop model and more realistic compressible liquid drop approach with Sly5 parameters at three different temperatures, 3, 5, and 8 MeV, from disassembly of $Z_0 = 75$, $A_0 = 168$ at constant free-out volume $6V_0$. The intermediate mass fragment (IMF) multiplicity ($M_{\rm IMF}$) is also an important observable in the nuclear multifragmentation process which is measured both experimentally and theoretically in many situations [35–41]. The IMF multiplicity ($M_{\rm IMF}$) dependence with temperature (from

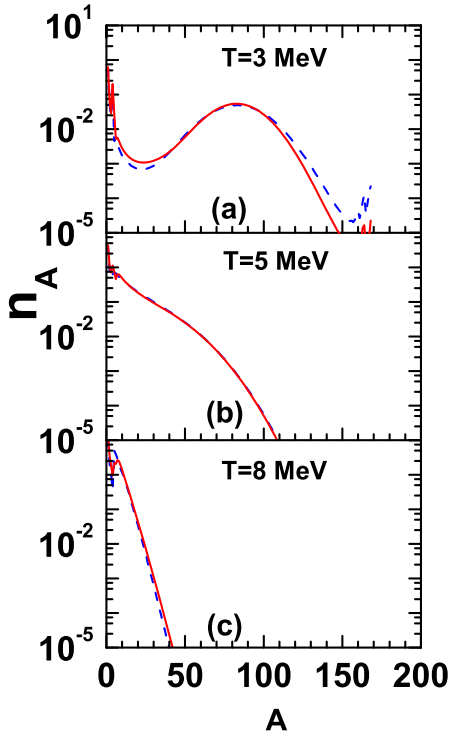

FIG. 2. Mass distribution from fragmentation of $Z_0 = 75$, $A_0 = 168$ system at temperature $T = 3$ MeV(upper panel), 5 MeV(middle panel), and 8 MeV(lower panel) studied from conventional CTM calculation (blue dashed lines) and CTM calculation with realistic Sly5 EoS (red solid lines).

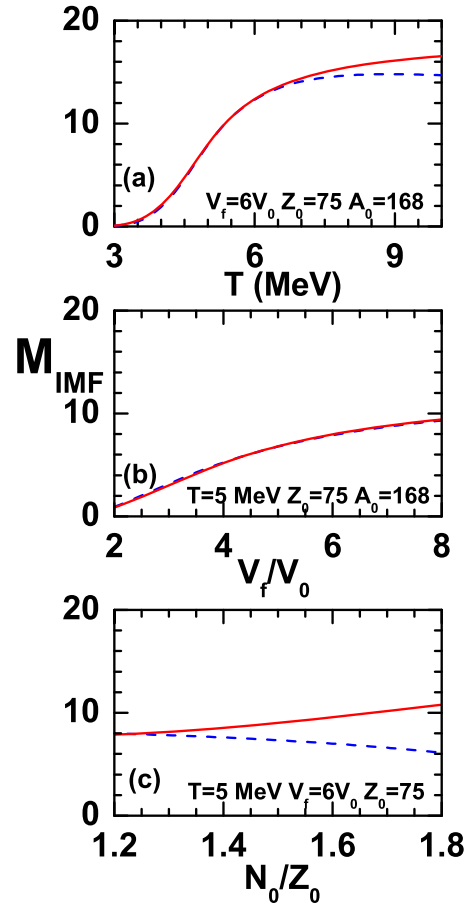

FIG. 3. Variation of multiplicity of intermediate mass fragments ($M_{\rm IMF}$) with (a) temperature (upper panel) and (b) freeze-out volume (middle panel) and isospin asymmetry of the fragmenting system (lower panel) from conventional CTM calculation (blue dashed lines) and CTM calculation with realistic Sly5 EoS (red solid lines). Calculations are performed for fragmenting system of atomic number $Z_0 = 75$ and mass number $A_0 = 168$.

disassembly of $Z_0 = 75, A_0 = 186$ at constant free-out volume $6V_0$), freeze-out volume (for the same fragmenting system $Z_0 = 75$, $A_0 = 168$ but at constant temperature 5 MeV), and neutron to proton ratio of the fragmenting system (from disassembly with constant $Z_0 = 75$ at constant temperature 5 MeV and free-out volume $6V_0$) are presented in Fig. 3. From Fig. 3, it can be verified that the effect of nuclear binding on intermediate mass fragment multiplicity is more significant at higher temperature and freeze-out volume, i.e., the conditions at which the system breaks more. For a given temperature and freeze-out volume, the IMF multiplicity is strongly modified for the fragmentation from very isospin asymmetric systems due to significant production of neutron rich nuclei. Figure 4 represents the isotopic distribution of some selective lower (helium), intermediate (carbon, oxygen, silicon, and calcium), and heavy (nickel) mass fragments originated from the multifragmentation of $Z_0 = 75$, $A_0 = 168$ system at temperature 5 MeV and free-out volume $6V_0$. As in the IMF region, neutron-rich isotopes are more bound in the compressible liquid drop approach with Sly5 parameters compared to the conventional liquid drop model, and hence the production of neutron-rich isotopes of carbon, oxygen, silicon, and calcium is significantly enhanced.

One of the important aspects of intermediate energy heavy ion reactions study is to reduce the uncertainty in the nuclear equation of state. Isoscaling [32,33,42–48] and isobaric yield ratio [47–51] methods are commonly used to search the precise nuclear equation of state. In this work, the effect of nuclear binding on isoscaling and isobaric yield ratio are investigated in the framework of CTM. It has been observed both experimentally and theoretically that the ratio of yields from two different reactions (having different isospin asymmetry) exhibit an exponential relationship as a function of the neutron (N) and proton (Z) number and this is termed as "isoscaling." Two fragmentation reactions 1 and 2 at a given energy are being considered whose fragmenting systems have different masses A_{01} and A_{02} ($A_{02} > A_{01}$) but same charge $Z_1 = Z_2 = Z_0$:

$$R_{21} = \langle n_{2N,Z}\rangle/\langle n_{1N,Z}\rangle = C\exp(\alpha N + \beta Z), \qquad (18)$$

where α and β are the isoscaling parameters and C is a normalization factor. Figure 5 represents the isoscaling ratios obtained from CTM calculation at constant temperature $T = 5$ MeV and freeze-out volume $V_f = 6V_0$ for two fragmenting sources with identical atomic numbers $Z_0 = 75$ but different mass numbers $A_{01} = 168$ and $A_{02} = 186$. The

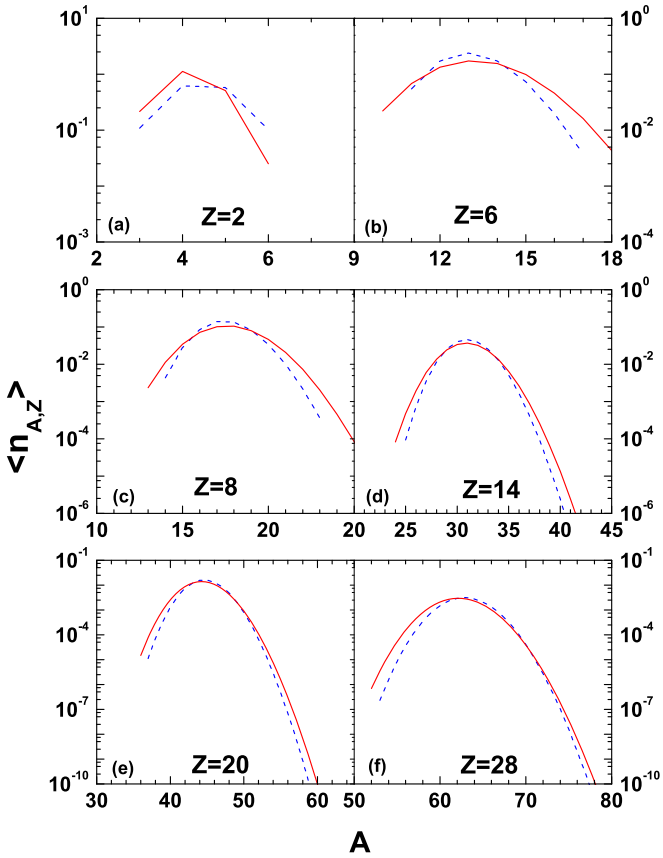

FIG. 4. Isotopic distributions for $Z = 2$, 6, 8,14, 20, and 28 from fragmentation of $Z_0 = 75$, $A_0 = 168$ system at $T = 5$ MeV studied from conventional CTM calculation (blue dashed lines) and CTM calculation with realistic Sly5 EoS (red solid lines).

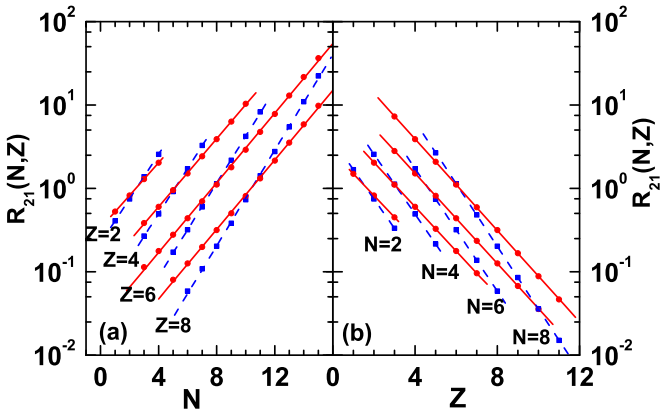

FIG. 5. Ratios (R_{21}) of multiplicities of fragments of producing the nucleus (N, Z) where system 1 is $Z_0 = 75$, $A_0 = 168$ and system 2 is $Z_0 = 75$, $A_0 = 186$. Conventional CTM results (blue dashed lines) are compared with CTM calculation with realistic Sly5 EoS (red solid lines). For each case reactions are simulated at constant temperature $T = 5$ MeV and freeze-out volume $V_f = 6V_0$. The left panel shows the ratios as function of neutron number N for fixed Z values, while the right panel displays the ratios as function of proton number Z for fixed neutron numbers. The lines drawn through the points are best fits of the calculated ratios.

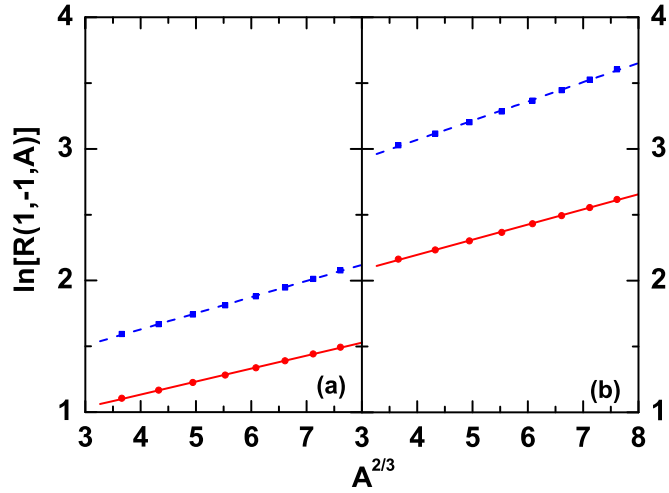

FIG. 6. Variation of isobaric yield ratio $\ln R[1, -1, A]$ with $A^{2/3}$ for $Z_0 = 75, A_0 = 168$ (left panel) and $Z_0 = 75, A_0 = 186$ (right panel) from the conventional CTM approach (blue dashed lines) and CTM calculation with realistic Sly5 EoS (red solid lines). Calculations are performed at temperature $T = 5$ MeV and freeze-out volume $V_f = 6V_0$.

isoscaling ratio R_{21} is plotted as function of the neutron number (N) for $Z = 2$, 4, 6, and 8 in the left panel whereas the right panel displays the ratio as function of the proton number (Z) for $N = 2$, 4, 6, and 8. The lines are the best fits of the calculated R_{21} ratios to Eq. (18). From Fig. 5, it can be concluded that CTM calculation with more realistic semi-microscopic binding and excitation also shows isoscaling behavior, but with the inclusion of realistic semi-microscopic binding the magnitude of the isoscaling parameters α and β decreased.

The isobaric ratio of yields [49] of two different types of fragments having same mass number A but different isospin asymmetry $I = N - Z$ and $I' = N' - Z'$ originating from the fragmenting system is given by

$$R[I', I, A] = \langle n_{I,A} \rangle / \langle n_{I',A} \rangle. \tag{19}$$

The quantity $R[I', I, A]$ shows linear behavior with $A^{2/3}$ for $I = 1$ and $I' = -1$ from the conventional liquid drop approach [48]. Figure 6 confirms that for semi-microscopic realistic binding this linear behavior also holds but for a given fragment mass number, production of neutron-rich isotopes is greater with realistic binding compared to the conventional liquid drop approach, and hence the isobaric yield ratio value is less. This reduction is more for fragmentation from more isospin asymmetric systems ($Z_0 = 75$ and $A_0 = 186$) compared to other one ($Z_0 = 75$ and $A_0 = 168$).

The excited fragments produced in the multifragmentation stage decay to their stable ground states. They can γ decay to shed energy but may also decay by light particle emission to lower mass nuclei. Hence, an evaporation model with the same realistic semi-microscopic binding and excitation is developed. Emissions of n, p, d, t, ^{3}He, and ^{4}He particles are considered. Particle-decay widths are obtained using Weisskopf's evaporation theory [52]. To study the cluster functional effect on cold fragments for isospin sensitive observables like isotopic distribution, isoscaling, and isobaric

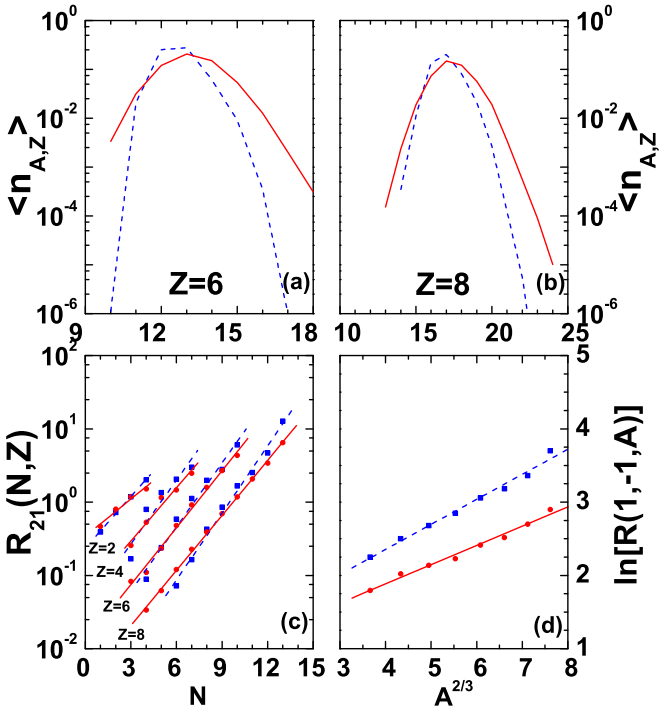

FIG. 7. Upper panels: Isotopic distributions for $Z = 6$ (upper left panel) and $Z = 8$ (upper right panel) after secondary decay from $Z_0 = 75$, $A_0 = 168$ system. Lower left panel: Ratios (R_{21}) of multiplicities of secondary fragments (N, Z) where system 1 is $Z_0 = 75, A_0 = 168$ and system 2 is $Z_0 = 75, A_0 = 186$. (The lines drawn through the points are best fits of the calculated ratios.) Lower right panel: Variation of isobaric yield ratio $\ln R[1, -1, A]$ of secondary fragments with $A^{2/3}$ for $Z_0 = 75, A_0 = 168$. Blue dashed lines represents results from the CTM calculation described in Sec. II- A followed by the evaporation model [18] with binding from the conventional liquid drop model and excitation from Fermi gas model, whereas red solid lines indicates results obtained from the CTM calculation described in Sec. II- B followed by the evaporation model with realistic binding and excitation. All calculations are performed at temperature $T = 5$ MeV and freeze-out volume $V_f = 6V_0$.

yield ratio, two separate cases are considered: (a) CTM calculation described in Sec. II A followed by the evaporation model [18,53] with binding from the conventional liquid drop model and excitation from the Fermi gas model, and (b) CTM calculation described in Sec. II B followed by the evaporation model with realistic binding and excitation. The results are presented in Fig. 7, which confirms relative enhancement of multiplicities of very neutron-rich isotopes and reduction of isoscaling parameters as well as isobaric yield ratio, due to the introduction of new cluster functionals that exist strongly even after secondary decay.

IV. SUMMARY AND FUTURE OUTLOOK

The canonical thermodynamical model of nuclear multifragmentation is upgraded with more realistic semi-microscopic binding and excitation. The bulk part of the binding is determined from newly proposed metamodeling of the equation of state with Sly5 parameters. The effect of the cluster functional has been examined for basic observables of nuclear multifragmentation like intermediate mass fragment multiplicity and mass distribution as well as isospin sensitive observables like isotopic distribution, isoscaling, and isobaric yield ratio at different thermodynamic conditions of temperature and freeze-out volume and isospin asymmetry of the fragmenting system which can be accessed in laboratory experiments. Semi-microscopic realistic binding significantly modifies intermediate mass fragment production (from isospin asymmetric fragmenting systems), multiplicity of neutron-rich isotopes, isoscaling and isobaric yield ratio parameters. These modifications due to inclusion of the realistic cluster functional are also present after the secondary decay of the excited fragments.

In a future work, it will be interesting to study the effect of different nuclear EoS of fragmentation observables in the framework of this upgraded statistical model. Hybrid model calculations are quite successful for explaining projectile fragmentation reactions in the limiting fragmentation region, but one of the major constraints of the presently available hybrid models is that the dynamical stage is performed with microscopic interaction where as fragmentation is treated with statistical models where conventional liquid drop binding and level density are used, therefore substantial error may arise due to this inconsistency during the coupling of the transport model output result and further statistical model calculation. This newly proposed CTM model will bypass such difficulty and can be coupled more efficiently with a dynamical model with identical interaction in both stages. It will be very interesting to pursue that in a future work.

ACKNOWLEDGMENTS

The author gratefully acknowledges F. Gulminelli of LPC Caen, G. Chaudhuri of VECC, and S. D. Gupta of McGill University for valuable discussions and suggestions.

[1] S. Das Gupta, S. Mallik and G. Chaudhuri, *Heavy Ion Reaction at Intermediate Energies: Theoretical Models* (World Scientific Publishers, Singapore, 2019).
[2] B.-A. Li and W.-U. Schroder, *Isospin Physics in Heavy-Ion Collisions at Intermediate Energies* (Nova Science, New York, 2001).
[3] P. J. Siemens, Nature (London) **305**, 410 (1983).
[4] D. H. E. Gross, Prog. Part. Nucl. Phys. **30**, 155 (1993).
[5] J. P. Bondorf, A. S. Botvina, A. S. Iljinov, I. N. Mishustin, and K. Sneppen, Phys. Rep. **257**, 133 (1995).
[6] S. Das Gupta, A. Z. Mekjian, and M. B. Tsang, in *Advances in Nuclear Physics*, Advances in the Physics of Particles and Nuclei, Vol. 26, edited by J. W. Negele and E. W. Vogt (Springer, Boston, MA, 2001), pp. 89–166.
[7] P. Chomaz, M. Colonna, and J. Randrup, Phys. Rep. **389**, 263 (2004).

[8] B. Borderie and M. F. Rivet, Prog. Part. Nucl. Phys. **61**, 551 (2008).
[9] B. Borderie and J. D. Frankland, Prog. Part. Nucl. Phys. **105**, 82 (2019).
[10] B.-A. Li, L.-W. Chen and C. M. Ko, Phys. Rep. **464**, 113 (2008).
[11] A. S. Botvina and I. N. Mishustin, Phys. Rev. C **72**, 048801 (2005).
[12] Ph. Chomaz, F. Gulminelli, C. Ducoin, P. Napolitani, and K. Hasnaoui, AIP Conf. Proc. **884**, 318 (2007)
[13] D. H. Gross, Phys. Rep. **279**, 119 (1997).
[14] J. Randrup and S. E. Koonin, Nucl. Phys. A **471**, 355 (1987).
[15] C. B. Das, S. Das Gupta, W. G. Lynch, A. Z. Mekjian, and M. B. Tsang, Phys. Rep. **406**, 1 (2005).
[16] H. A. Bethe and R. F. Bacher, Rev. Mod. Phys. **8**, 82 (1936).
[17] C. F. v. Weizsöcker, Z. Phys. **96**, 431 (1935).
[18] G. Chaudhuri and S. Mallik, Nucl. Phys. A **849**, 190 (2011).
[19] K. C. Chase and A. Z. Mekjian, Phys. Rev. C **52**, R2339 (1995).
[20] N. Alam, G. Chaudhuri, and F. Gulminelli, Phys. Rev. C **102**, 064620 (2020).
[21] S. Mallik and F. Gulminelli, Phys. Rev. C **103**, 015803 (2021).
[22] F. Gulminelli and Ad. R. Raduta, Phys. Rev. C **92**, 055803 (2015).
[23] J. Margueron, R. Hoffmann Casali, and F. Gulminelli, Phys. Rev. C **97**, 025805 (2018).
[24] E. Chabanat, P. Bonche, P. Haensel, J. Meyer, and R. Schaeffer, Nucl. Phys. A **635**, 231 (1998).
[25] P. Papakonstantinou, J. Margueron, F. Gulminelli, and A. R. Raduta, Phys. Rev. C **88**, 045805 (2013).
[26] T. Carreau, F. Gulminelli, and J. Margueron, Eur. Phys. J. A **55**, 188 (2019).
[27] T. Carreau, F. Gulminelli, and J. Margueron, Phys. Rev. C **100**, 055803 (2019).
[28] J. M. Lattimer and F. Douglas Swesty, Nucl. Phys. A **535**, 331 (1991).
[29] INDRA collaboration, J. D Frankland, B Borderie, M Colonna, M. F Rivet, Ch. O. Bacri, Ph. Chomaz, D. Durand, A. Guarnera, M. Pârlog, M Squalli *et al.*, Nucl. Phys. A **689**, 940 (2001).
[30] H. S. Xu, M. B. Tsang, T. X. Liu, X. D. Liu, W. G. Lynch, W. P. Tan, A. Vander Molen, G. Verde, A. Wagner, H. F. Xi *et al.*, Phys. Rev. Lett. **85**, 716 (2000).
[31] T. X. Liu, M. J. van Goethem, X. D. Liu, W. G. Lynch, R. Shomin, W. P. Tan, M. B. Tsang, G. Verde, A. Wagner, H. F. Xi *et al.*, Phys. Rev. C **69**, 014603 (2004).
[32] W. P. Tan, B.-A Li, R. Donangelo, C. K. Gelbke, M.-J. van Goethem, X. D. Liu, W. G. Lynch, S. Souza, M. B. Tsang, G. Verde, A. Wagner and H. S. Xu, Phys. Rev. C **64**, 051901(R) (2001).
[33] S. Mallik and G. Chaudhuri, Nucl. Phys. A **1002**, 121948 (2020).
[34] M. Wang, W. J. Huang, F. G. Kondev, G. Audi, and S. Naimi, Chin. Phys. C **45**, 030003 (2021).
[35] G. F. Peaslee, M. B. Tsang, C. Schwarz, M. J. Huang, W. S. Huang, W. C. Hsi, C. Williams, W. Bauer, D. R. Bowman, M. Chartier, J. Dinius, C. K. Gelbke, T. Glasmacher, D. O. Handzy, M. A. Lisa, W. G. Lynch, C. M. Mader, L. Phair, M. C. Lemaire, S. R. Souza, G. VanBuren, R. J. Charity, L. G. Sobotka, G. J. Kunde, U. Lynen, J. Pochodzalla, H. Sann, W. Trautmann, D. Fox, R. T. deSouza, G. Peilert, W. A. Friedman, and N. Carlin, Phys. Rev. C **49**, R2271(R) (1994).
[36] C. A. Ogilvie, J. C. Adloff, M. Begemann-Blaich, P. Bouissou, J. Hubele, G. Imme, I. Iori, P. Kreutz, G. J. Kunde, S. Leray *et al.*, Phys. Rev. Lett. **67**, 1214 (1991).
[37] M. B. Tsang, W. C. Hsi, W. G. Lynch, D. R. Bowman, C. K. Gelbke, M. A. Lisa, G. F. Peaslee, G. J. Kunde, M. L. Begemann-Blaich, T. Hofmann *et al.*, Phys. Rev. Lett. **71**, 1502 (1993).
[38] R. Ogul, A. S. Botvina, U. Atav, N. Buyukcizmeci, I. N. Mishustin, P. Adrich, T. Aumann, C. O. Bacri, T. Barczyk, R. Bassini *et al.*, Phys. Rev. C **83**, 024608 (2011).
[39] S. Mallik, G. Chaudhuri, and S. Das Gupta, Phys. Rev. C **84**, 054612 (2011).
[40] S. Mallik, G. Chaudhuri, P. Das, and S. Das Gupta, Phys. Rev. C **95**, 061601(R) (2017).
[41] P. Das, S. Mallik, and G. Chaudhuri, Phys. Lett. B **783**, 364 (2018).
[42] M. B. Tsang, W. A. Friedman, C. K. Gelbke, W. G. Lynch, G. Verde, and H. S. Xu, Phys. Rev. Lett. **86**, 5023 (2001).
[43] A. S. Botvina, O. V. Lozhkin and W. Trautmann, Phys. Rev. C **65**, 044610 (2002).
[44] G. Chaudhuri, S. Das Gupta, and M. Mocko, Nucl. Phys. A **813**, 293 (2008).
[45] M. Colonna, Phys. Rev. Lett. **110**, 042701 (2013).
[46] A. R. Raduta and F. Gulminelli, Phys. Rev. C **75**, 024605 (2007).
[47] S. Mallik and G. Chaudhuri, Phys. Rev. C **87**, 011602(R) (2013).
[48] S. Mallik and G. Chaudhuri, Phys. Lett. B **727**, 282 (2013).
[49] M. Huang, Z. Chen, S. Kowalski, Y. G. Ma, R. Wada, T. Keutgen, K. Hagel, M. Barbui, A. Bonasera, C. Bottosso *et al.*, Phys. Rev. C **81**, 044620 (2010).
[50] S. R. Souza and M. B. Tsang, Phys. Rev. C **85**, 024603 (2012).
[51] C. W. Ma, F. Wang, Y. G. Ma, and C. Jin, Phys. Rev. C **83**, 064620 (2011).
[52] V. Weisskopf, Phys. Rev. **52**, 295 (1937).
[53] S. Mallik, Ph.D. thesis (Chapter II), Homi Bhabha National Institute (2016), arXiv:2009.00283.